RSC Advances

PAPER

View Article Online
View Journal | View Issue

Cite this: *RSC Adv.*, 2021, **11**, 3295

The colorimetric and microfluidic paper-based detection of cysteine and homocysteine using 1,5-diphenylcarbazide-capped silver nanoparticles†

Sattar Shariati and Gholamreza Khayatian *

We have prepared a microfluidic paper-based analytical device (μPAD) for the determination of cysteine and homocysteine based on 1,5-diphenylcarbazide-capped silver nanoparticles. The μPAD was developed to identify and quantify the levels of cysteine and homocysteine. The proposed μPAD enabled the detection of cysteine and homocysteine using a colorimetric reaction based on modified silver nanoparticles. The color of the modified AgNPs in the test zone immediately changed after the addition of cysteine and homocysteine. Based on this change, the quantification of these two amino acids was achieved using an RGB color model and ImageJ software. Under optimized conditions, the proposed device enabled the determination of cysteine in the 0.20–20.0 μM concentration range with a limit of detection (LOD) of 0.16 μM. In addition, the LOD of homocysteine was calculated to be 0.25 μM with a linear range of 0.50–20.0 μM. In this work, we focused on the use of the μPAD for the analysis of a series of human urine samples.

Received 10th October 2020
Accepted 21st December 2020

DOI: 10.1039/d0ra08615k

rsc.li/rsc-advances

Introduction

The aminothiols, such as cysteine (Cys), homocysteine (Hcy), and glutathione (GSH), play essential metabolic roles in physiological and pathological processes. For example, Cys plays a vital role in the structure of proteins, and their synthesis and function.[1,2] Cys can effect many functions including the normal growth rate of hair, the growth rate in children, reduce the effects of aging on the skin, liver health, and the growth of muscle. In addition, Cys may help burn fat and increase muscle mass.[3] Several studies have indicated that an abnormal level of cysteine is directly linked to many diseases, including Parkinson's disease, Alzheimer's disease, and adverse pregnancy outcomes.[4,5]

Hcy is an intermediate generated during the synthesis of Cys from the essential amino acid (methionine).[6] The level of Hcy can be used to predict the rate of prevalence of heart disease, apoplexy, and Alzheimer's disease, as well as acting as an independent indicator of heart, brain, and peripheral vascular diseases.[7,8] In addition to the above-mentioned thiols, thiol drugs such as D-penicillamine (D-PEN or Pena)[9] and tiopronin (TP or Thiola),[10] are also widely used in clinical practice. The quantitative detection of these drugs and their metabolites is very important in related clinical research.

Therefore, the detection of Cys and Hcy is very important. At present, plenty of detection techniques have been explored to detect biothiols, including high performance liquid chromatography (HPLC),[11] mass-spectrometry,[12] chemiluminescence,[13] electrochemistry,[14] fluorescence spectroscopy,[15,16] capillary electrophoresis,[17] gas chromatography (GC),[18,19] and so on. Although these methods allow the sensitive detection of biothiols, the complicated preparation process and expensive instrumentation limits their application. Colorimetric sensing strategies using plasmonic nanomaterials are usually based on a change in the optical properties owing to changes in their aggregation and morphology.[20–22] Colorimetric methods have been successfully employed for the analysis of several analytes, including metal ions and biothiols.[23]

Microfluidic paper-based analytical devices (μPADs) have grown rapidly over the past decade. In recent years, μPADs have been developed for quantitative analysis and applied in medical fields, healthcare and environmental monitoring. The main purpose of fabricating μPADs is to provide a low-cost, simple design and environmentally friendly analytical chemistry tool, which is suitable for use in the field.[24–27] Several methods have been reported for the fabrication of μPADs including photolithography,[28] wax printing,[29] wet-etching,[30] and so on. In the wet-etching method, trimethoxyoctadecylsilane-heptane (TMOS-heptane) solution is used to create a hydrophilic-hydrophobic pattern on filter paper. In this work, we used a wet-etching method using siloxane solution to create hydrophobic walls that aqueous solutions cannot easily cross. This method could be used in any lab at a minimum cost.

Department of Chemistry, Faculty of Science, University of Kurdistan, P.O. Box 416, Sanandaj, Iran. E-mail: gkhayatian@uok.ac.ir; Fax: +98 873 3624133; Tel: +98 9181719609

† Electronic supplementary information (ESI) available. See DOI: 10.1039/d0ra08615k

The fabrication of μPADs was developed using diphenylcarbazide-capped silver nanoparticles. Diphenylcarbazide is an organic compound commonly used as an indicator for titrating iron and for the colorimetric determination of Cr(VI). Liu *et al.* have reported a colorimetric method for the detection of Cr(VI) using gold nanoparticles (AuNPs) modified using the reagent 1,5-diphenylcarbazide (DPC).[31] DPC has two amino groups that may react on the surface of the nanoparticles through hydrogen bonding interactions. In this work, we used DPC as a selective ligand to modify silver nanoparticles for the determination of Cys and Hcy in real samples.

Experimental

Reagents and materials

$AgNO_3$, $NaBH_4$, DPC, triethoxymethylsilane (TEMS), $NaHCO_3$, Na_2CO_3, ethanol, nitric acid (65%) and polyvinyl pyrrolidone (PVP), were purchased from Merck (Darmstadt, Germany, www.merck.com). Alanine (Ala), arginine (Arg), asparagine (Asn), aspartic acid (Asp), cysteine (Cys), homocysteine (Hcy), glutamic acid (Glu), glutamine (Gln), glycine (Gly), histidine (His), isoleucine (Ile), leucine (Leu), lysine (Lys), methionine (Met), phenylalanine (Phe), proline (Pro), serine (Ser), threonine (Thr), tryptophan (Trp), tyrosine (Tyr), and valine (Val) were purchased from Merck Company. Stock solutions of $AgNO_3$ and $NaBH_4$ were prepared by dissolving a suitable amount of $AgNO_3$ and $NaBH_4$ in deionized water. Doubly distilled deionized water was used in all the experiments.

Apparatus

The UV-Vis absorption data were recorded on a DR5000 spectrophotometer (Hach, United States of America). A digital pH-Meter (sension 378, Hach, U.S) was used for the pH measurements. All the photographs in the experiments were taken using a Sony digital camera and mobile camera. All captured images were analyzed with RGB values using the image scientific software ImageJ, ver.1.46r, developed by the National Health Institute, USA (available at http://imagej.nih.gov/ij).

Synthesis of the modified silver nanoparticles

The AgNPs were prepared by reducing $AgNO_3$ with sodium borohydride in aqueous solution by varying the concentration of the reducing agent.[32] A 5.0 mL solution of 1.0 mM silver nitrate was added dropwise (about 1 drop per second) to 45 mL of freshly prepared 0.06 M sodium borohydride solution that had been chilled in an ice bath. The reaction mixture was stirred vigorously on a magnetic stirrer plate for 20 min until the solution turned light yellow. For the preparation of the DPC–AgNPs, the AgNPs (50 mL) were incubated with 5.0 mL of 1.0 mM DPC aqueous solution under stirring at room temperature for 1 h. The DPC–AgNPs were stored at 4 °C and remained stable for 3 months.

Fabrication of μPADs

Scheme 1(A–C) shows the fabrication principles and process. Firstly, a pattern designed using Coreldraw 2019 software was printed onto a filter paper with a LaserJet printer (Canon i-sensys LBP6030w). The pattern design was cut with a sharp knife along the printed pattern on the filter paper (Scheme 1A). The remaining mold was then immersed in a 10% (v/v) TEMS–ethanol solution for 10 s. The TEMS–ethanol solution (10% (v/v)) was used as a patterning agent for salinization of the hydrophilic filter paper, it was removed and air dried for 1 min, then it was heated at 100 °C for 1 h in an oven (Scheme 1B). After

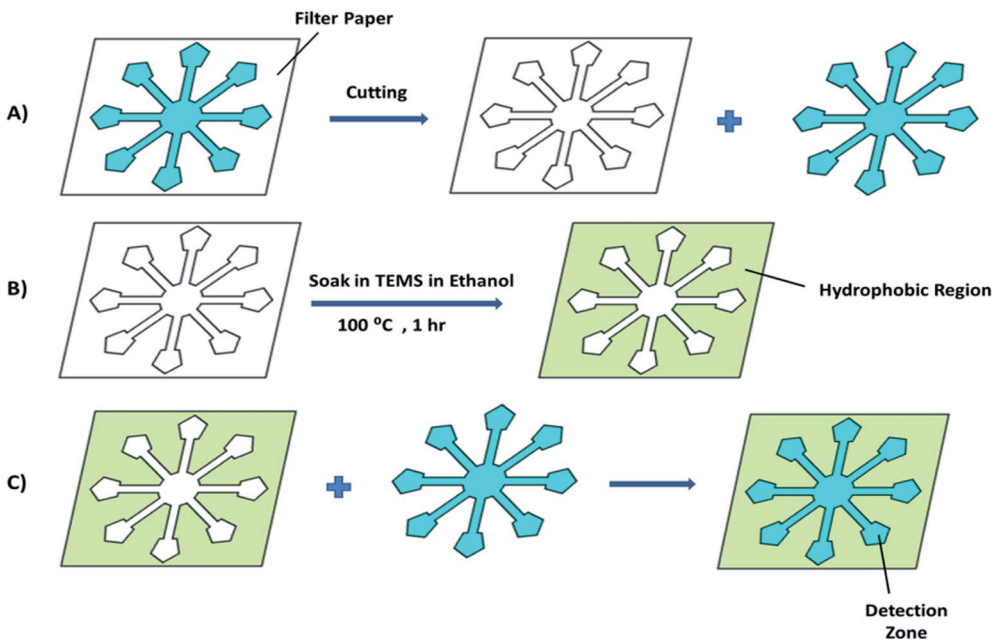

Scheme 1 A schematic diagram showing the fabrication of the μPADs.

that, the hydrophobic pattern was returned to the original location (Scheme 1C). As a result, a hydrophilic–hydrophobic contrast was generated on the filter paper.

Results and discussion

Colorimetric detection of cysteine

The pH of the DPC–AgNPs was adjusted to 9.0 using carbonate/bicarbonate (0.01 M) buffer solution using a pH meter. Then, Cys and Hcy were added separately with concentrations ranging from 0.20 to 25.0 μM and 0.50–20 μM, respectively. In the presence of Cys and Hcy, the color of the solutions changed from light yellow to pink during the 1 min incubation time. For the UV-Vis spectra and microfluidic paper-based analytical device measurements, the required sample volumes were 1.0 mL and 10 μL, respectively. Under the optimum experimental conditions, the calibration curve was found to be linear over the range of 0.20–25.0 μM for Cys with a detection limit of 0.14 μM (Fig. 1). Meanwhile, the calibration curve was found to be linear over the range of 0.50–20.0 μM for Hcy with a detection limit of 0.22 μM (Fig. 2).

A designed flower-shaped microfluidic paper-based analytical device (μPAD) was used for the Cys and Hcy assays. The μPAD consists of 8 channels, 8 detection zones and 1 central unit. Fig. 3 shows an image of the Cys assay on the μPAD for the standard samples. The procedure for Cys or Hcy sensing using the μPAD is described as follows, 50 μL of DPC–AgNPs solution was dropped into the middle of the hydrophilic central unit on the μPAD. After that, 10 μL of the solutions at various concentration of Cys or Hcy were added into the hydrophilic detection zones separately. After drying, images of the μPADs were captured using a Sony digital camera or mobile camera. All captured images were analyzed using RGB values and ImageJ 1.46r software or a color picker app and then the mean gray value for each test zone was determined. The yellow color of the loaded μPADs gradually changed to a pink color upon the addition of Cys or Hcy. The ratio of the color intensity of each detection zone is related to the Cys or Hcy concentration in the

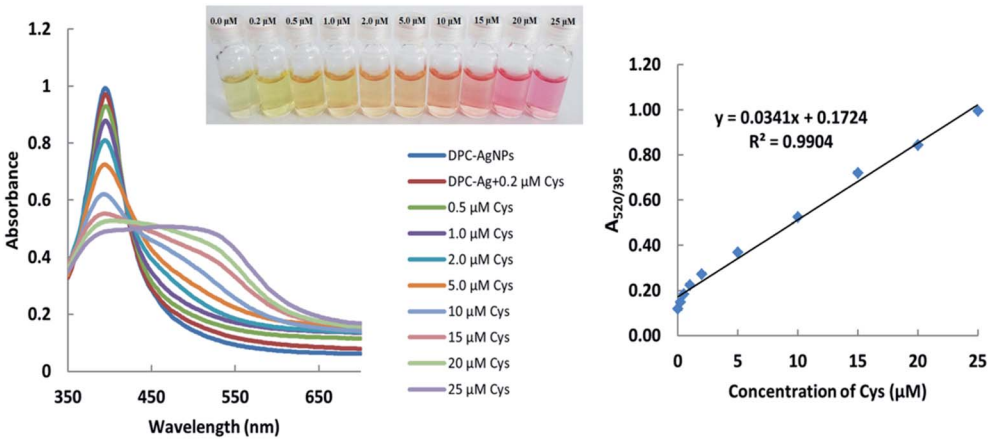

Fig. 1 Absorption spectra and absorption ratios ($A_{520/395}$) of the DPC–AgNPs solution after the addition of different concentrations of cysteine.

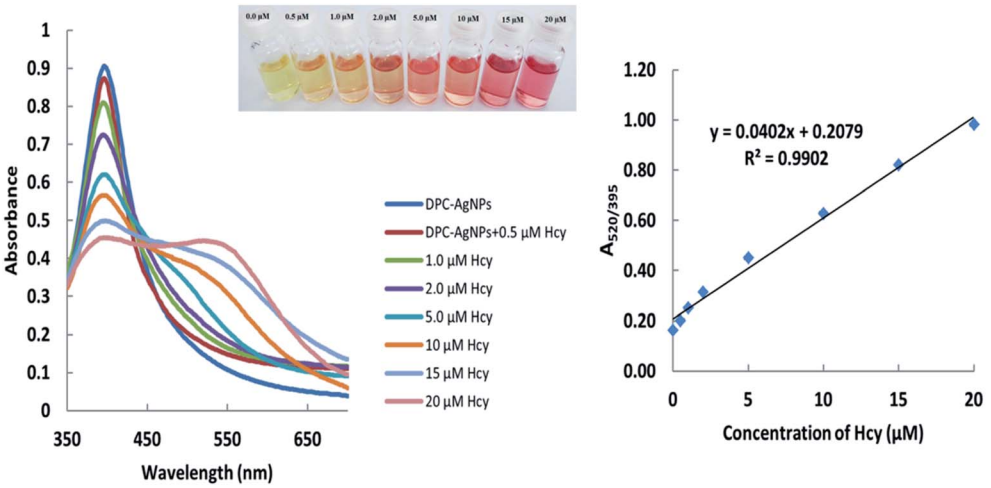

Fig. 2 Absorption spectra and absorption ratios ($A_{520/395}$) of the DPC–AgNPs solution after the addition of different concentrations of homocysteine.

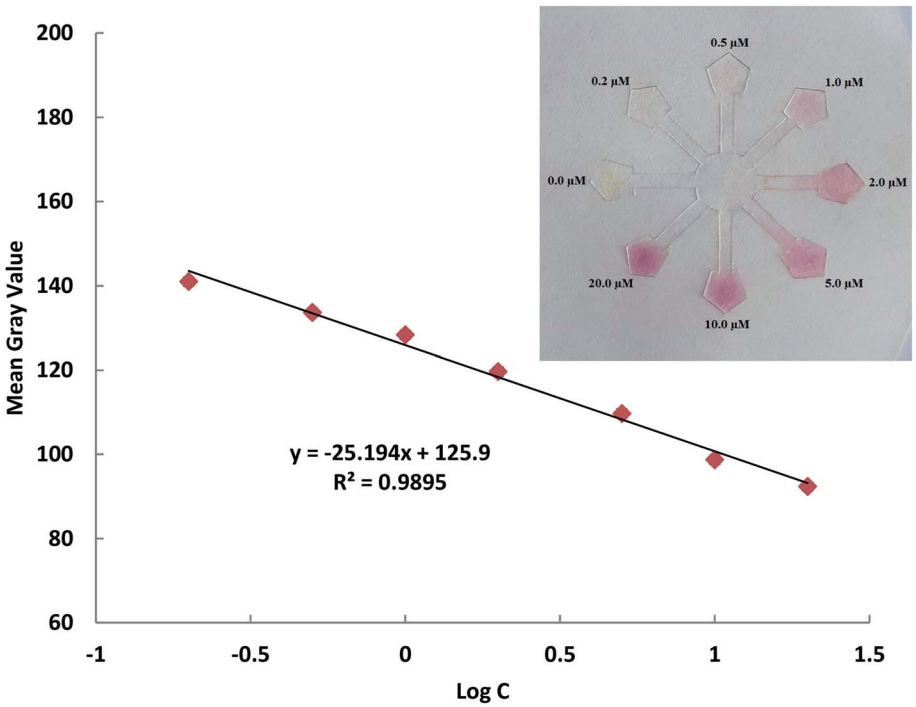

Fig. 3 The detection of Cys using DPC–AgNPs on the μPAD in the presence of different concentrations of Cys in the range of 0.20–20.0 μM and the linear calibration of the color ratio *versus* log C.

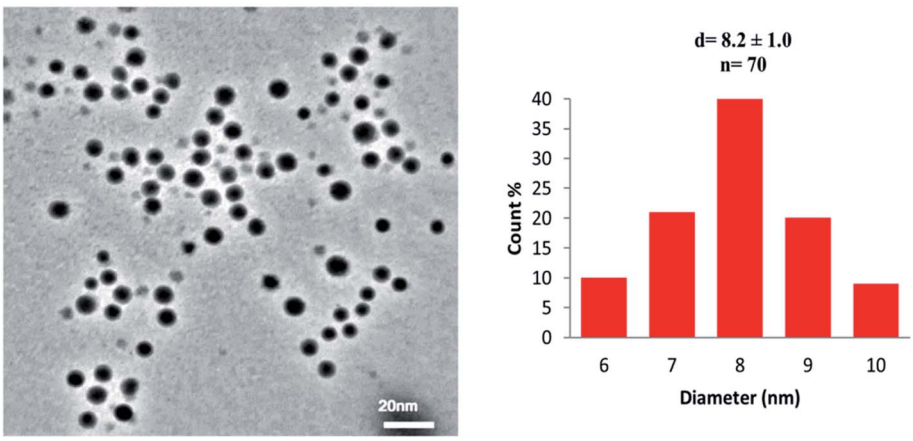

Fig. 4 A TEM image of DPC–AgNPs and the size-range histogram.

solutions. The linear correlation of cysteine was obtained between the RGB intensity ratio *versus* the log C in the range of 0.20–20.0 μM with a correlation coefficient (R^2) of 0.98, and a LOD of 0.16 μM for the μPAD (Fig. 3). In the case of Hcy, a linear correlation was obtained in the range of 0.50–20 μM with a correlation coefficient (R^2) of 0.98, and a LOD of 0.25 μM.

The transmission electron microscopy (TEM) images and histogram demonstrate the DPC–AgNPs are well-dispersed (Fig. 4). As shown in the TEM image, the DPC–AgNPs are spherical and well dispersed in the aqueous solution with an average size of 8.2 ± 1.0 nm for $n = 70$. The TEM image of DPC–AgNPs in the presence of 10 μM Cys shows that the DPC–AgNPs aggregated to form large particles (Fig. 5).

Selectivity of the DPC–AgNPs

The selectivity of the proposed platform was tested in aqueous solutions with different types of ions. Solutions containing 20.0 μM Cys or Hcy and 200 μM of other amino acids, including Ala, Arg, Asn, Asp, Gln, Gly, Glu, His, Ile, Leu, Lys, Met, Phe, Pro, Thr, Trp, Tyr, Val and Ser, were used as the target analytes. The experiments were carried out in aqueous solution (Fig. 6) and using the μPAD (Fig. 7). The novel μPAD were designed and used for this purpose (μPAD had 10 points without any channels). As

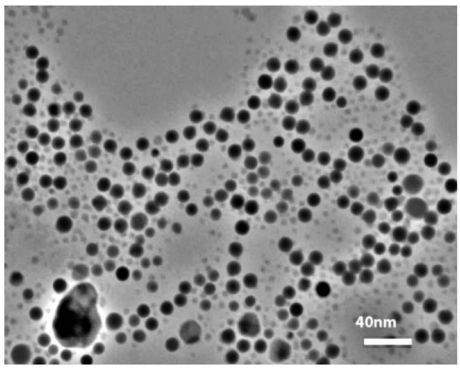

Fig. 5 A TEM image of DPC–AgNPs in the presence of 10 μM Cys.

can be clearly seen in Fig. 6 and 7, the proposed method is selective for the determination of Cys or Hcy, even at concentrations that are 10 times lower than the other amino acids.

This selectivity is due to the fact that DPC contains two amino groups and one oxygen atom that can attach onto the surface of the silver nanoparticles through two Ag–NH_2 and Ag–O bonds, see Fig. S1 (ESI†).

The bonding status of DPC on the surface of the Ag nanoparticles was characterized using FT-IR spectroscopy and the results are shown in Fig. S2.† In the infrared spectra of DPC, the strong peak at 1710 cm^{-1} is attributed to the C=O stretching vibration. The peaks at 732, 796, 3097 and 3330 cm^{-1} are attributed to the wagging and stretching vibrations of the –NH groups in DPC. When DPC was coated onto the surface of the AgNPs, the carboxylic peak was shifted from 1710 to 1627 cm^{-1} and the peaks of the amine groups expanded and disappeared. A comparison of the two spectra of pure DPC and DPC–AgNPs shows that the DPC has attached onto the AgNPs. The decrease in the peak intensity of the C=O stretching bond and the shift to 1616 cm^{-1} may be due to the interaction of Cys with the DPC–AgNPs. After the addition of Cys or Hcy, the nanoparticles

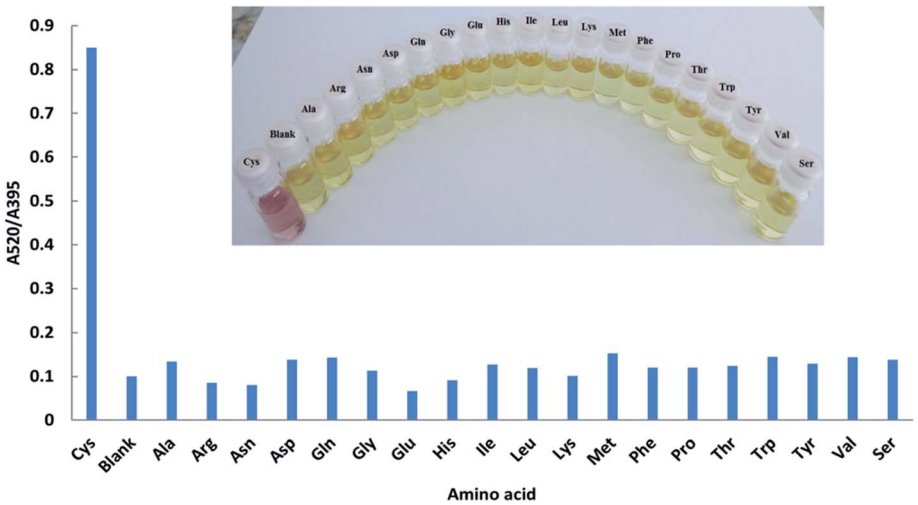

Fig. 6 Absorption ratios ($A_{520/395}$) of DPC–AgNPs with 20.0 μM Cys and 200 μM various amino acids at pH = 9.0.

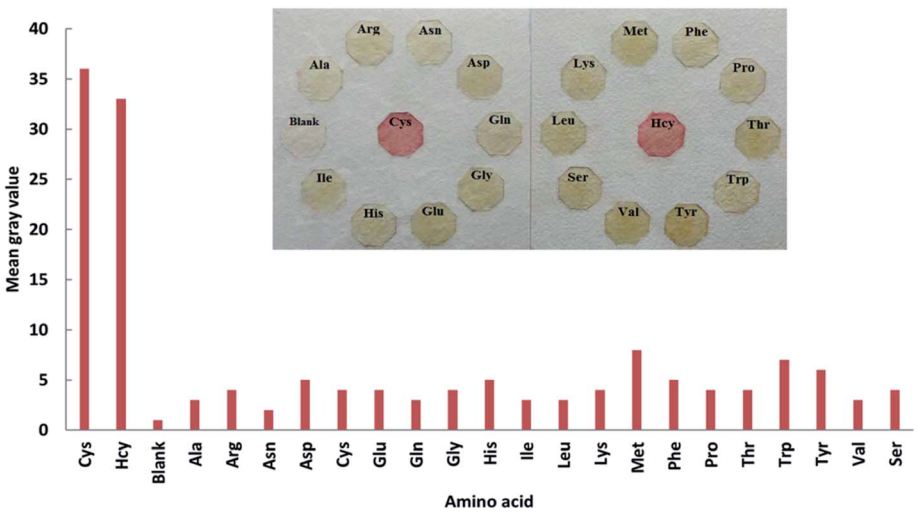

Fig. 7 Selectivity testing of the μPAD in the presence of Cys and Hcy (20.0 μM) and other amino acids (200 μM).

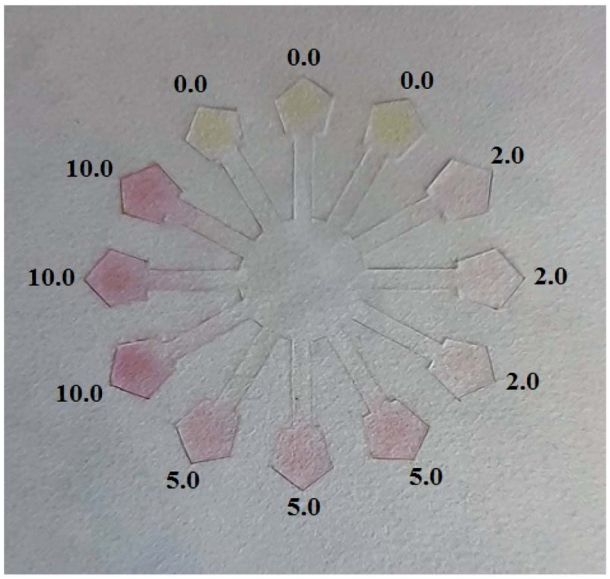

Fig. 8 Results of Cys and Hcy detection in human urine samples using the μPAD.

become close to each other by a cross-linking mechanism through the two hydrogen bonds of the COO^- and $-NH_2$ groups and this induces the aggregation of the AgNPs (Fig. S2 in the ESI†). The other amino acids that do not have sulfur atoms cannot attach themselves to the nanoparticles and do not induce any noticeable responses to DPC–AgNP.

Analysis of real samples

To show the efficiency of this colorimetric probe, the concentrations of Cys and Hcy were determined in human urine samples. The urine samples were diluted with distilled water prior to analysis to obtain similar concentrations of the matrix compounds in all samples. The human urine samples were spiked with known concentrations of Cys and Hcy at different levels (Fig. 8).

The results are listed in Table 1. The results were obtained before and after the addition of the same mixture of the Cys and Hcy standards in equal volumes to the urine samples. Then, the percentage recovery was calculated by comparison of the results. For each test, two independent samples were used for all procedures and each sample was analyzed three times. As can be seen, the average recovery for the determination of Cys and Hcy was very good for both methods (UV-Vis and μPADs).

Table 1 Recoveries of Cys and Hcy, with equal volumes added to human urine samples

Method	Urine sample	Added (μM)	Found (μM) ($n = 3$)	Recovery%	Average%	RSD (%) ($n = 3$)
UV-Vis spectroscopy (DR5000)	1	0.0	—	—	—	—
		2.0	1.95, 2.06, 2.11	97.5, 103.0, 111.0	103.8	4.0
	2	5.0	5.08, 5.27, 5.35	101.6, 105.4, 107.0	104.6	2.6
		10.0	10.02, 10.17, 10.31	100.2, 101.7, 103.1	101.7	1.4
Proposed method (μPAD)	1	0.0	—	—	—	—
		2.0	2.12, 2.17, 2.30	106.0, 108.5, 115.0	109.8	4.2
	2	5.0	5.05, 5.22, 5.40	101.0, 104.4, 108.0	104.5	3.3
		10.0	10.05, 10.30, 10.48	100.5, 103.0, 104.8	102.7	2.1

Table 2 A comparison of different methods for the determination of cysteine and homocysteine

Method	Nanomaterial	Range (μM)	LOD (μM)	Ref.
Chemiluminescence	Silver nanoclusters	0.005–1.0	0.0025	13
Fluorescence probe	DEX–AgNPs	0.0–6.0	0.0016	16
UV-vis spectroscopy	PVP-stabilized AgNPs	3.2–8.2	2.8	33
UV-vis spectroscopy	Citrate–AgNPs	1.0–150	1.5	34
UV-vis spectroscopy	Chitosan–AgNPs	Cys: 0.5–10	Cys: 0.015	35
		Hcy: 0.1–5.0	Hcy: 0.0846	
UV-vis spectroscopy	DNA–AuNPs	0.05–10	0.1	36
Colorimetry (near-infrared fluorescence)	Copper complex	10–40	4.0	37
UV-vis spectroscopy	DEX–AgNPs	100–1000	12.0	38
UV-vis spectroscopy	PAN–Cu^{2+} complex	2.25 - 42.91	38.0	39
UV-vis and PAD	TMB–Ag^+ complex	4–290	2.46	40
UV-vis spectroscopy	Chitosan–AuNPs	0.1–30	0.1	41
UV-vis spectroscopy	DPC–AgNPs	Cys: 0.2–25.0	Cys: 0.14	This work
		Hcy: 0.5–20	Hcy: 0.22	
μPAD smartphone	DPC–AgNPs	Cys: 0.2–20.0	Cys: 0.16	This work
		Hcy: 0.5–20	Hcy: 0.25	

Therefore, this μPAD platform is suitable for quantifying Cys and Hcy concentrations.

In Table 2, the analytical performances of this method were compared with some of the previous methods used for the determination of Cys and Hcy.[13,16,33–41] The results show that the method has a lower LOD and a wider linear dynamic range than the other reported methods. Also, this method has a broader linear range and a shorter response time.

Conclusions

In the present study, a simple and sensitive colorimetric method for the detection of Cys and Hcy was established. Silver nanoparticles were synthesized *via* the reduction of $AgNO_3$ with $NaBH_4$, which were modified using DPC. As a novel platform, DPC–AgNPs were used for the detection of trace amounts of Cys and Hcy in the presence of different interfering amino acids. The DPC–AgNPs solution exhibited high colorimetric selectivity toward Cys and Hcy. The assay results indicated that the aggregation of the colloidal solutions could be enhanced in the presence of Cys or Hcy, displaying changes in the color and the UV-vis absorbance spectra. The mechanism of aggregation is based on the interaction of the donating groups of DPC with these two amino thiols. Thus, an exceptionally simple and rapid method for detecting Cys or Hcy was obtained. This method shows good linearity between the absorbance ratio ($A_{520/395}$) and the concentration of Cys and Hcy in the range of 0.20–25.0 μM and 0.50–20.0 μM, respectively. The relative coefficient for both of these is 0.99. Also, this mechanism could be successfully used based on a μPAD in the linear range of 0.20–20.0 μM for Cys and 0.50–20 μM for Hcy with a relative coefficient of 0.98. The present method was successfully used to determine the concentrations of Cys and Hcy in human urine samples. This approach offers several advantages, including the rapid application the method, easy detection of the end result by the naked eye in the presence of different amino acids, and low cost, owing to the use of simple instruments.

Conflicts of interest

There are no conflicts to declare.

Acknowledgements

The authors are grateful for financial support for this study from the University of Kurdistan, Grant Number (2018).

References

1 Y. Tang, L. Jin and B. Yin, A dual-selective fluorescent probe for GSH and Cys detection: Emission and pH dependent selectivity, *Anal. Chim. Acta*, 2017, **993**, 87–95, DOI: 10.1016/j.aca.2017.09.028.

2 L. He, Q. Xu, Y. Liu, H. Wei, Y. Tang and W. Lin, A coumarin based turn-on fluorescence probe for specific detection of glutathione over cysteine and homocysteine, *ACS Appl. Mater. Interfaces*, 2015, **23**, 12809–12813, DOI: 10.1021/acsami.5b01934.

3 S. H. Xue, S. S. Ding, Q. S. Zhai, H. Y. Zhang and G. Q. Feng, A readily available colorimetric and near-infrared fluorescent turn-on probe for rapid and selective detection of cysteine in living cells, *Biosens. Bioelectron.*, 2015, **68**, 316–321, DOI: 10.1016/j.bios.2015.01.019.

4 S. Shahrokhian, Lead phtalocyanine as a selective carrier for preparation of a cysteine-selective electrode, *Anal. Chem.*, 2001, **73**(24), 5972–5978, DOI: 10.1021/ac010541m.

5 M. T. Heafield, S. Fearn, G. B. Steventon, R. H. Waring, A. C. Williams and S. G. Sturman, Plasma cysteine and sulphate levels in patients with motor neurone, Parkinson's and Alzheimer's disease, *Neurosci. Lett.*, 1990, **110**(1–2), 216–220, DOI: 10.1016/0304-3940(90)90814-p.

6 K. S. McCully, Homocysteine metabolism, atherosclerosis, and diseases of aging, *Compr. Physiol.*, 2016, **6**(1), 471–505.

7 K. Miwa, M. Tanaka, S. Okazaki, Y. Yagita, M. Sakaguchi, H. Mochizuki and K. Kitagawa, Increased total Homocysteine levels predict the risk of incident dementia independent of cerebral Small-Vessel diseases and vascular risk factors, *J. Alzheimer's Dis.*, 2015, **49**(2), 503–513.

8 Z. Fu, X. Hao and J. Guo, Hyperhomocysteinemia is an independent predictor of long-term clinical outcomes in Chinese octogenarians with acute coronary syndrome, *Clin. Interventions Aging*, 2015, **10**, 1467–1474.

9 J. Peisach and W. E. Blumberg, A mechanism for the action of penicillamine in the treatment of Wilson's disease, *Mol. Pharmacol.*, 1969, **5**, 200–209.

10 J. G. Zhang and W. E. Lindup, Tiopronin protects against the nephrotoxicity of cisplatin in rat renal cortical slices in vitro, *Toxicol. Appl. Pharmacol.*, 1996, **141**, 425–433.

11 G. Chwatko, E. Kuzniak, P. Kubalczyk, K. Borowczyk, M. Wyszczelska-Rokiela and R. Głowacki, Determination of cysteine and glutathione in cucumber leaves by HPLC with UV detection, *Anal. Methods*, 2014, **6**, 8039–8044, DOI: 10.1039/c4ay01574f.

12 Y. F. Huang and H. T. Chang, Nile Red-Adsorbed Gold Nanoparticle Matrixes for Determining Aminothiols through Surface-Assisted Laser Desorption/Ionization Mass Spectrometry, *Anal. Chem.*, 2006, **78**(5), 1485–1493, DOI: 10. 1021/ac0517646.

13 X. J. Yu, Q. J. Wang, X. N. Liu and X. L. Luo, A sensitive chemiluminescence method for the determination of cysteine based on silver nanoclusters, *Microchim. Acta*, 2012, **179**, 323–328, DOI: 10.1007/s00604-012-0893-3.

14 K. K. Aswini, A. M. Vinu Mohan and V. M. Biju, Molecularly imprinted polymer based electrochemical detection of L-cysteine at carbon paste electrode, *Mater. Sci. Eng., C*, 2014, **37**, 321–326, DOI: 10.1016/j.msec.2014.01.020.

15 F. Gao, Q. Q. Ye, P. Cui, X. X. Chen, M. G. Li and L. Wang, Selective ''turn-on'' fluorescent sensing for biothiols based on fluorescence resonance energy transfer between acridine orange and gold nanoparticles, *Anal. Methods*, 2011, **3**, 1180–1185, DOI: 10.1039/c1ay05073g.

16 X. Liu, W. Zhang, Ch. Li, W. Zhou, Zh. Li, M. Yu and L. Wei, Nanomolar detection of Hcy, GSH and Cys in aqueous

solution, test paper and living cells, *RSC Adv.*, 2015, **5**, 4941–4946, DOI: 10.1039/c4ra13262a.

17 P. Kubalczyk, E. Bald, P. Furmaniaka and R. Głowacki, Simultaneous determination of total homocysteine and cysteine in human plasma by capillary zone electrophoresis with pH-mediated sample stacking, *Anal. Methods*, 2014, **6**, 4138–4143, DOI: 10.1039/c4ay00287c.

18 L. Chen, D. L. Capone and D. W. Jeffery, Analysis of Potent Odour-Active Volatile Thiols in Foods and Beverages, *Molecules*, 2019, **24**(13), 2472–2496, DOI: 10.3390/molecules24132472.

19 Q. Wang, J. M. Chong and J. Pawliszyn, Determination of thiol compounds by automated headspace solid-phase, *Flavour Fragrance J.*, 2006, **21**, 385–394, DOI: 10.1002/ffj.1724.

20 M. Ma, J. Wang and X. Zheng, Enhancement of the colorimetric sensitivity of gold nanoparticles with triethanolamine to minimize interparticle repulsion, *Microchim. Acta*, 2010, **172**(1–2), 155–162, DOI: 10.1007/s00604-010-0480-4.

21 Z. J. Li, X. J. Zheng, L. Zhang, R. P. Liang, Z. M. Li and J. D. Qiu, Label-free colorimetric detection of biothiols utilizing SAM and unmodified Au nanoparticles, *Biosens. Bioelectron.*, 2015, **68**, 668–674, DOI: 10.1016/j.bios.2015.01.062.

22 S. K. Vaishnav, C. K. Patel, J. Korram, R. Nagwanshi, K. K. Ghosh and M. L. Satnami, Surface plasmon resonance based spectrophotometric determination of medicinally important thiol compounds using unmodified silver nanoparticles, *Spectrochim. Acta, Part A*, 2017, **179**, 155–162, DOI: 10.1016/j.saa.2017.02.040.

23 P. Ni, Y. Sun, H. Dai, J. Hu, S. Jiang, Y. Wang and Z. Li, Highly sensitive and selective colorimetric detection of glutathione based on Ag [I] ion–3,3′,5,5′-tetramethylbenzidine (TMB), *Biosens. Bioelectron.*, 2015, **63**, 47–52, DOI: 10.1016/j.bios.2014.07.021.

24 A. K. Yetisen, M. S. Akram and C. R. Lowe, Paper-based microfluidic point-of-care diagnostic devices, *Lab Chip*, 2013, **13**, 2210–2251, DOI: 10.1039/c3lc50169h.

25 A. W. Martinez, S. T. Phillips, M. J. Butte and G. M. Whitesides, Patterned paper as a platform for inexpensive, low-volume, portable bioassays, *Angew. Chem., Int. Ed.*, 2007, **46**, 1318–1320, DOI: 10.1002/anie.200603817.

26 Y. Xu, M. Liu, N. Kong and J. Liu, Lab-on-paper micro- and nano-analytical devices: Fabrication, modification, detection and emerging applications, *Microchim. Acta*, 2016, **183**(5), 1521–1542, DOI: 10.1007/s00604-016-1841-4.

27 S. Faham, G. Khayatian, H. Golmohammadi and R. Ghavami, A paper-based optical probe for chromium by using gold nanoparticles modified with 2,2′-thiodiacetic acid and smartphone camera readout, *Microchim. Acta*, 2018, **185**(8), 374–381, DOI: 10.1007/s00604-018-2875-6.

28 W. Dungchai, O. Chailapakul and C. S. Henry, Use of multiple colorimetric indicators for paper-based microfluidic devices, *Anal. Chim. Acta*, 2010, **674**(2), 227–233, DOI: 10.1016/j.aca.2010.06.019.

29 E. Carrilho, A. W. Martinez and G. M. Whitesides, Understanding Wax Printing: A Simple Micropatterning Process for Paper-Based Microfluidics, *Anal. Chem.*, 2009, **81**(16), 7091–7095, DOI: 10.1021/ac901071p.

30 L. Cai, Y. Wang, Y. Wu, C. Xu, M. Zhong, H. Lai and J. Huang, Fabrication of a microfluidic paper-based analytical device by silanization of filter cellulose using a paper mask for glucose assay, *Analyst*, 2014, **139**, 4593–4598, DOI: 10.1039/c4an00988f.

31 L. Liu, Y. Leng and H. Lin, Photometric and visual detection of Cr(VI) using gold nanoparticles modified with 1,5-diphenylcarbazide, *Microchim. Acta*, 2016, **183**(4), 1367–1373, DOI: 10.1007/s00604-016-1777-8.

32 L. Mulfinger, S. D. Solomon, M. Bahadory, A. V. Jeyarajasingam, S. A. Rutkowsky and C. Boritz, Synthesis and Study of Silver Nanoparticles, *J. Chem. Educ.*, 2007, **84**(2), 322–325, DOI: 10.1021/ed084p322.

33 F. Bamdad, F. Khorram, M. Samet, K. Bamdad, M. R. Sangi and F. Allahbakhshi, Spectrophotometric determination of L-cysteine by using polyvinylpyrrolidone-stabilized silver nanoparticles in the presence of barium ions, *Spectrochim. Acta, Part A*, 2016, **161**, 52–57, DOI: 10.1016/j.saa.2016.02.030.

34 S. K. Vaishnav, K. Patel, K. Chandraker, J. Korram, R. Nagwanshi, K. K. Ghosh and M. L. Satnami, Surface plasmon resonance based spectrophotometric determination of medicinally important thiol compounds using unmodified silver nanoparticles, *Spectrochim. Acta, Part A*, 2017, **179**, 155–162, DOI: 10.1016/j.saa.2017.02.040.

35 S. Mohammadi and G. Khayatian, Colorimetric detection of biothiols based on aggregation of chitosan-stabilized silver nanoparticles, *Spectrochim. Acta, Part A*, 2017, **185**, 27–34, DOI: 10.1016/j.saa.2017.05.034.

36 J. S. Lee, P. A. Ulmann, M. S. Han and C. A. Mirkin, A DNA-gold nanoparticle-based colorimetric competition assay for the detection of cysteine, *Nano Lett.*, 2008, **8**(2), 529–533, DOI: 10.1021/nl0727563.

37 W. Hao, A. McBride, S. McBride, J. P. Gao and Z. Y. Wang, Colorimetric and near-infrared fluorescence turn-on molecular probe for direct and highly selective detection of cysteine in human plasma, *J. Mater. Chem.*, 2011, **21**(4), 1040–1048, DOI: 10.1039/c0jm02497j.

38 S. Davidovic, V. Lazic, I. Vukoje, J. Papan, S. P. Anhrenkiel, S. Dimitrijevic and J. M. Nedeljkovic, Dextran coated silver nanoparticles-Chemical sensor for selective cysteine detection, *Colloids Surf., B*, 2017, **160**, 184–191, DOI: 10.1016/j.colsurfb.2017.09.031.

39 G. Deilamy-Rad, K. Asghari and H. Tavallali, Development of a Reversible Indicator Displacement Assay Based on the 1-(2-Pyridylazo)-2-naphthol for Colorimetric Determination of Cysteine in Biological Samples and Its Application to Constructing the Paper Test Strips and a Molecular-Scale Set/Reset Memorized Device, *Appl. Biochem. Biotechnol.*, 2020, **192**, 85–102, DOI: 10.1007/s12010-019-03165-0.

40 Z. Xue, L. Xiong, H. Rao, X. Liu and X. Lu, A naked-eye liquid-phase colorimetric assay of simultaneous detect cysteine

and lysine, *Dyes Pigm.*, 2019, **160**, 151–158, DOI: 10.1016/j.dyepig.2018.07.054.
41 E. Jeyasekaran and S. Venkatachalam, Colorimetric detection of cysteine based on dispersion - aggregation of chitosan stabilized gold nanoparticles, *Can. J. Chem.*, 2018, 1–13, DOI: 10.1139/cjc-2018-0258.